Received: 26 January 2021 | Revised: 28 May 2021 | Accepted: 4 June 2021

IET Generation, Transmission & Distribution

DOI: 10.1049/gtd2.12294

The Institution of Engineering and Technology WILEY

ORIGINAL RESEARCH PAPER

Fault current compensations in resonant grounded distribution systems to mitigate powerline bushfires using a nonsingular terminal sliding model controller

Tushar Kanti Roy[1,2] | **Md Apel Mahmud**[2]

[1] Department of Electronics & Telecommunication Engineering, Rajshahi University of Engineering and Technology, Rajshahi, Bangladesh

[2] Electrical Power & Energy Systems Research Lab (EPESRL), School of Engineering, Deakin University, Waurn Ponds, Australia

Correspondence
Tushar Kanti Roy, Department of Electronics, and Telecommunication Engineering, Rajshahi University of Engineering and Technology, Rajshahi-6204, Bangladesh, Electrical Power & Energy Systems Research Lab (EPESRL), School of Engineering, Deakin University, Waurn Ponds, VIC 3216, Australia.
Email: tkroy@ete.ruet.ac.bd

Abstract

A fault current compensation technique is proposed in this paper for resonant grounded power distribution systems in bushfire prone areas. Arc suppression devices with residual current compensation inverters are used to compensate fault currents due to single line-to-ground faults in order to mitigate powerline bushfires. The main contribution of this paper is the design of a compensation technique for the T-type residual current compensation inverter using a non-singular terminal sliding mode control scheme. The main objective of the proposed scheme is to reduce the fault current and bring its value to a level so that it cannot ignite fires. The proposed controller is designed based on the selection of a sliding surface in a way the singularity problem can be avoided and chattering effects in existing sliding mode controllers can be eliminated. The desired current injection through the residual current compensation inverter is ensured by enforcing the control law into the terminal sliding surface where the control law is determined by satisfying the Lyapunov stability criteria. The performance of the non-singular terminal sliding mode controller is compared with an integral sliding mode controller by considering different values of fault currents where these values are varied by changing fault resistances. Results for simulation in the software and processor-in-loop simulations are verified against operational standards which are essential for mitigating powerline bushfires. This work focuses to design a non-singular terminal sliding mode controller for the residual current compensation inverter which is used in an arc suppression device to compensate both active and reactive components of the fault current and keeps its value below 0.5 A within 2 s after activating the residual current compensation inverter which is a requirement as per the operational standard. This controller is designed based on the selection of a terminal sliding surface while satisfying the condition for avoiding the singularity problem.

1 | INTRODUCTION

Power distribution networks are generally grounded to compensate currents due to electric faults as high fault currents ignite fires. There are different grounding techniques and resonant grounding techniques are considered as the most feasible solutions to compensate fault currents for power distribution networks in bushfire prone areas [1]. In resonant grounded power distribution systems (RGPDSs), arc suppression devices (ASDs) with adjustable inductor coils are connected between the neutral and ground which are automatically adjusted to compensate fault currents by making resonance with the available zero-sequence capacitance at the substation when there are single line-to-ground (SLG) faults in RGPDSs [2].

The resonant grounding with ASDs helps to protect the network assets and enhance the safety of the overall system [3]. However, the resonant condition assists to compensate only the reactive component of the fault current though its active component can be significant enough to start powerline bushfires. For this reason, ASDs are equipped with residual current

compensation (RCC) inverters which inject current to the neutral point to fully compensate the fault current or reduce its value to a lower value. Generally, the requirement for mitigating powerline bushfires the fault current needs to be kept at a value below 0.5 A within 2 s after initiating the action of the RCC inverter [4]. This clearly indicates that the RCC inverter needs to act quickly to compensate the fault current. Furthermore, the fault current significantly varies as it depends on the fault resistance. Therefore, it is essential to regulate the output current of the RCC inverter with variations in fault resistances which is a challenging task as the regulation capability relies on the switching control actions. This challenge for the fault current compensation in RGPDSs can be overcome by appropriately designing controllers for the RCC inverter.

Several model-free controllers are used to compensate the fault current in resonant controllers where these controllers are mainly designed based on proportional integral (PI) control schemes. PI controllers are generally used for reducing the tracking error for the desired control objective. For the RCC inverter in the ASD, the key task is to reduce the fault current either by tracking the neutral current or faulty phase voltage. A closed-loop control structure using a PI controller is presented in [5, 6] for compensating the fault current in transmission networks. However, the controller in [6] provides compensation only for the active component with an assumption that the adjustable inductor fully compensates the reactive component which does not actually happen in practice. Although the PI controller in [5] shows some improvements in the performance as it uses advanced topologies, transmission lines are designed with more safety features, these lines are not much responsible for igniting fires while comparing with distribution networks.

Different types of PI controllers are employed for RCC inverters to compensate the fault current in distribution networks which include single- or dual-loop configurations where some of these schemes have compound characteristics, that is, more than one controller is used within a single-loop in order to improve the performance. The single-loop structures are proposed in [7, 8] where the main task of these controllers is to reduce the current flowing through the fault impedance either by tracking the faulty phase voltage or neutral current. These simple model-free controllers use the PI control scheme to track the sinusoidal reference. The compound controllers for the RCC inverter are designed in [9, 10] in which more than one controller is used within a loop for compensating the fault current in order to improve the performance over the simple PI controllers. The controller in [9] works based on open- and closed-loop compound structures with PI controllers. However, the approach in [9] requires the measurement of insulation parameters for the pre-set control parameters. In [10], a distributed commutation scheme is used in conjunction with a PI controller. Although the controller in [10] shows some improvements in the tracking performance, it requires additional communication schemes and suffers from the delay. Furthermore, all these PI controllers suffer from steady-state tracking errors even after utilising advanced modulation techniques as these aim to track the sinusoidal reference. A segmented proportional integral derivative (PID) controller is used in [11] for compensating the overshoots in the current and voltage during the grid synchronisation rather maintaining the operational standard for mitigating powerline bushfires. A model-based proportional resonant (PR) controller is used in [12] in consecution with a PI controller by forming a compound structure within a single-loop configuration. Although the PI+PR controller improves the damping and enhances the stability margin, this scheme still experiences significant tracking errors along with the requirement for satisfying some strict conditions [12]. An advanced model-based H_∞ controller is proposed in [13] where the order of the controller becomes unrealistic which makes it difficult for the practical implementation even after applying the order reduction technique. Another model-based model predictive controller is presented in [14] for compensating the fault current. However, this controller is designed for low impedance faults though the main challenge for compensating the fault current in an RGPDS system is the high impedance fault.

The RCC inverter can be controlled by dual-loop control structures with an outer voltage control loop and an inner current control loop. Here, the outer loop can be used to generate the reference of the current to be controlled by controlling the neutral voltage and the inner loop current controller then controls the current for compensating the fault current in a way that the risk of powerline bushfires are significantly reduced. It is worth noting that the dual-loop structure reduces the risk of bushfires in faster way as compared to other existing model-free controllers as one control loop (i.e. the outer loop) is used to generate the reference current and other control loop regulate the current to follow the reference. Thus, the response time is faster which in turn reduces the risk of bushfires. Several dual-loop controllers are used in [15–17] including compound structures. In [15], PI controllers are used for both loops, whereas a lag compensator is employed in [16] for the outer loop and a PI controller for the inner loop. Similarly, the outer loop in [17] uses a compound control structure with a PI+PR controller while the inner loop utilises a proportional (P) controller. Although the fault current compensation is improved with these controllers, there are still some problems such as the tracking error for the sinusoidal reference with a PI controller and high steady-state errors with the P controller. The control schemes so far discussed in this work are limited to operating points, that is, these controllers compensate the fault current for some specific fault resistances.

Non-linear controllers have been successfully employed in many power system applications as these controllers ensure desired performance over a range of operating scenarios [18, 19]. Non-linear backstepping controllers ensure the desired tracking of the state as these are designed by satisfying the global stability criteria for the system [20]. The non-linear backstepping controllers are proposed in [21, 22] for the RCC inverters in ASDs to compensate the fault current while providing robustness against parametric uncertainties. However, these backstepping controllers consider uncertainties in the filter inductances which do not have significant effects on the overall performance of the system. Apart from this, these backstepping controllers do not exhibit any inherent properties to ensure the desired performance. Sliding mode controllers (SMCs)

have inherent capabilities to provide robustness against changes in operating conditions including parametric uncertainties and external disturbances [23]. The majority of these sliding mode controllers are desired based on higher order integral sliding surfaces which suffer from singularity problems and experience chattering. However, non-singular terminal SMCs (NT-SMCs) overcome the singularity problems of integral SMCs (I-SMCs) [24, 25]. A linear matrix inequality (LMI)-based finite-time SMC is proposed in [26] by proposing a new reaching law for uncertain non-linear systems. A sliding mode disturbance observer is proposed in [27] for the adaptive synchronisation in a fractional-order chaotic system. The finite-time chaos synchronisation based on the SMC is applied on for the secure communication in wireless sensor networks [28] and mobile communications [29]. However, none of these SMCs are employed for compensating the fault current using the RCC inverter in an ASD. Recently, a non-singular fast terminal sliding mode controller is proposed in [30] and a global terminal adaptive sliding mode controller is proposed in [31] which require additional parameters for ensuring the fast convergence. If this parameter is not selected properly, the controller in [30] cannot ensure the fast convergence of the tracking error.

Based on the existing literature, it can be summarised that the RCC inverter in an RGPDS system is mainly controlled to reduce the fault current without satisfying the required standard for compensating the powerline bushfire due to the single-line-to-ground faults. Although the recent works in [30, 31] consider the operational standard for powerline bushfire, it requires a number of design parameters that need to be selected appropriately to ensure the fast convergence. However, the selection of these parameters requires prior knowledge of the system and their inappropriate values affect the convergence. On the other hand, the fault current compensation needs to be performed within a specific timeframe. Hence, the severity of such a problem will be reduced if the number of such design parameters reduces. Moreover, the faults in power networks are considered as external disturbances that can easily be tackled through sliding mode controllers. These are considered as the main motivation for this work.

The main contribution of this work is to design an NT-SMC for the RCC inverter which is used in an ASD to compensate both active and reactive components of the fault current and keeps its value below 0.5 A within 2 s after activating the RCC inverter which is a requirement as per the operational standard as indicated in [4]. To the best of the authors' knowledge, this type of controller is not designed for the RCC inverter. An important feature of this controller is the selection of a terminal sliding surface for the RCC inverter that satisfies the condition for avoiding the singularity problem. The switching signals of the RCC inverter, which are used to regulate its output, are obtained in such a way that the tracking error is forced into this sliding surface and the concept of the control Lyapunov function (CLF) is used to ensure the global stability of the system. This has been further evidenced through the reachability analysis. The performance of the proposed NT-SMC is compared with an I-SMC and for this reason, a brief overview for designing the I-SMC is also included in this paper. Finally, simulation results are carried out by considering different values of the fault resistance in order to ensure the fault current compensation capability of the designed controller with variations in the fault current along with its superiority over the I-SMC. Simulation results from the software and processor-in-loop (PIL) clearly justify theoretical claims while satisfying the operational standard under all operating scenarios.

2 | DYNAMIC MODEL OF ASDs WITH RCC INVERTERS

Figure 1 shows an RGPDS having an ASD with a T-type RCC inverter in which the distribution substation is supplying a three-phase balanced load and an adjustable inductor (L_p) is connected between the neutral and ground. The ASD automatically adjusts this inductor when there is an SLG fault. At this instant, the switch S_N is also turned on to activate the T-type RCC inverter for compensating the fault current and it is connected through a step up transformer to match the output voltage with the neutral-to-ground voltage (v_N). The RCC inverter is used for injecting current to the neutral and compensates the fault current (i_f). The switches (S_1, S_2, S_3, and S_4) in this RCC inverter are controlled to regulate the neutral current (i_N) depending on the amount of the fault current that needs to be compensated where this value relies on the fault resistance. For this current compensation, the neutral current is used to determine the reference ($i_{N_{\text{ref}}}$) which is selected in such a way that the fault current becomes zero and this reference value is calculated from the expression of the neutral current. Figure 1 shows the impedance network for each phase where a resistance and a capacitance are connected in parallel. This figure also shows that an SLG fault is applied on Phase B. The current flowing through the neutral is calculated by using currents flowing through the fault resistance and zero-sequence impedance network in each phase which can be written as

$$i_N = i_f + i_S, \tag{1}$$

where $i_S = i_{A\sum} + i_{B\sum} + i_{C\sum}$ with $i_{A\sum}$, $i_{B\sum}$, and $i_{C\sum}$ as currents flowing through zero-sequence impedance networks in Phases A, B, and C, respectively. Here, the current flowing through the impedance network in each phase can be calculated as follows:

$$\begin{aligned} i_{A\sum} &= i_{R_{0A}} + C_{0A}\frac{dv_{C_{0A}}}{dt} = \frac{v_{C_{0A}}}{R_{0A}} + C_{0A}\frac{dv_{C_{0A}}}{dt} \\ i_{B\sum} &= i_{R_{0B}} + C_{0B}\frac{dv_{C_{0B}}}{dt} = \frac{v_{C_{0B}}}{R_{0B}} + C_{0B}\frac{dv_{C_{0B}}}{dt} \\ i_{C\sum} &= i_{R_{0C}} + C_{0C}\frac{dv_{C_{0C}}}{dt} = \frac{v_{C_{0C}}}{R_{0C}} + C_{0C}\frac{dv_{C_{0C}}}{dt}, \end{aligned} \tag{2}$$

where $i_{R_{0A}}$, $i_{R_{0B}}$, and $i_{R_{0C}}$ are currents flowing through the zero-sequence resistances in Phases A, B, and C, that, R_{0A}, R_{0B}, and R_{0C}, respectively; C_{0A}, C_{0B}, and C_{0C} are the zero-sequence

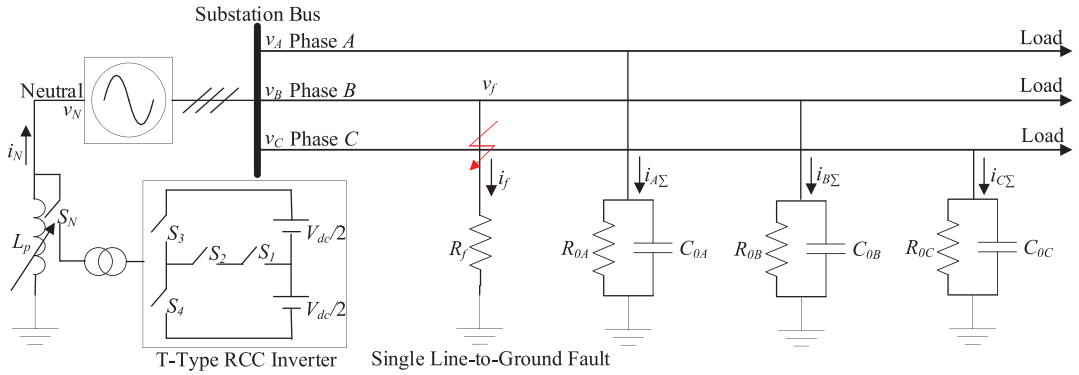

FIGURE 1 An RGPDS with a T-type RCC inverter in an ASD, having an SLG fault on Phase *B*

capacitances in Phases *A*, *B*, and *C*, respectively; and $v_{C_{0A}}$, $v_{C_{0B}}$, and $v_{C_{0C}}$ are voltages across C_{0A}, C_{0B}, and C_{0C}, respectively. Here, $v_{C_{0A}} = v_A$, $v_{C_{0B}} = v_B$, and $v_{C_{0C}} = v_C$. For a balanced distribution network, $R_{0A} = R_{0B} = R_{0C} = R_0$ and $C_{0A} = C_{0B} = C_{0C} = C_0$. Hence, Equation (2) can be simplified as

$$\begin{aligned} i_A\Sigma &= \frac{v_A}{R_0} + C_0\frac{dv_A}{dt} \\ i_B\Sigma &= \frac{v_B}{R_0} + C_0\frac{dv_B}{dt} \\ i_C\Sigma &= \frac{v_C}{R_0} + C_0\frac{dv_C}{dt}. \end{aligned} \tag{3}$$

Similarly, the fault current can be written as

$$i_f = \frac{v_f}{R_f} = \frac{v_B}{R_f}, \tag{4}$$

where v_f is the faulty phase voltage, which is also the phase-to-ground voltage for Phase *B* (i.e. v_B) as the fault is applied on this phase. Using Equation (3), i_S can be written as follows:

$$i_S = \frac{v_A + v_B + v_c}{R_0} + C_0\frac{d}{dt}(v_A + v_B + v_c). \tag{5}$$

The phase-to-neutral and neutral-to-ground voltages can be used to obtain the phase voltage which can be written as

$$\begin{aligned} v_A &= e_A + v_N \\ v_B &= e_B + v_N \\ v_C &= e_C + v_N, \end{aligned} \tag{6}$$

where e_A, e_B, and e_C are phase-to-neutral voltages for Phases *A*, *B*, and *C*, respectively. Since the system is considered as a balanced one, $e_A + e_B + e_C = 0$ for which Equation (6) can be simplified as

$$v_N = \frac{v_A + v_B + v_C}{3}. \tag{7}$$

Using the value of v_N from Equation (7), the simplified form of Equation (5) can be obtained as

$$i_S = 3\frac{v_N}{R_0} + 3C_0\frac{dv_N}{dt}. \tag{8}$$

Substituting Equations (4) and (8) into Equation (1), one can write:

$$i_N = \frac{v_B}{R_f} + 3\frac{v_N}{R_0} + 3C_0\frac{dv_N}{dt}. \tag{9}$$

The reference value of the neutral current can be calculated from Equation (9). The value of v_N needs to be expressed in terms of v_B and e_B based on Equation (6) as the SLG fault occurs on this phase. Hence, it can be written as

$$v_N = e_B - v_B \tag{10}$$

The substitution of Equation (10) into Equation (9) will yield:

$$\begin{aligned} i_N = &\left(\frac{3}{R_0} + \frac{1}{R_f}\right)v_B + 3C_0\frac{dv_B}{dt} \\ &- \left(\frac{3}{R_0}e_B + 3C_0\frac{de_B}{dt}\right). \end{aligned} \tag{11}$$

In Equation (11), i_f will be zero if $i_{N-\text{ref}}$ is selected as follows [22]:

$$i_{N_{\text{ref}}} = -\left(\frac{3}{R_0}e_B + 3C_0\frac{de_B}{dt}\right) \tag{12}$$

The changes in the current through the adjustable inductor can be expressed as follows:

$$\frac{di_N}{dt} = \frac{mV_{dc} - v_N}{L_p} \tag{13}$$

where m is the switching control signal that is used to regulate the current injection by the RCC inverter and V_{dc} is the input DC voltage to the RCC inverter. This modulation index is varied to track the reference current in Equation (12) by considering Equation (13) as the controlled plant. A NT-SMC is used in this paper to regulate the output current of the RCC inverter which is discussed in the following section.

3 | CONTROLLER DESIGN FOR RCC INVERTERS

As a NT-SMC is employed for the RCC inverter to compensate the fault current and its performance is compared with an I-SMC, this section discusses the complete design process for the NT-SMC along with an overview of the I-SMC. The proposed NT-SMC for the RCC inverter is designed based on the theoretical concept as presented in [24, 25] and it is worth mentioning that this scheme is not applied for controlling ASDs in RGPDSs to compensate the fault current. The detailed controller design process is discussed in the following subsections.

3.1 | Design of a NT-SMC for the RCC inverter in ASDs

A nonlinear terminal sliding surface is first chosen to design the NT-SMC which increases the convergence speed of the error and it can be defined as follows [24, 25]:

$$S_{NT-SMC} = \dot{e} + k_1 e^{\frac{p}{q}} \tag{14}$$

where S_{NT-SMC} is the terminal sliding surface; $e = i_N - i_{N_{\text{ref}}}$ is the tracking error; k_1 is a positive constant which is used to control the convergence speed of the error; and p and q represent positive odd numbers that need to be selected by satisfying the condition, $q < p < 2q$ in order to avoid the singularity problem [24, 25].

When the tracking error will reach at any point on the proposed terminal sliding surface as indicated by Equation (14) for any given initial conditions, the tracking error dynamic will be stable and reach to an equilibrium point within a finite time. Since the key control objective is to track the desired output, that is, the neutral current in RGPDSs for the application in this paper; the sliding mode control law will enforce the tracking error into the sliding surface for which $S_{NT-SMC} = 0$. With this condition, Equation (14) can be written as

$$\dot{e} = -k_1 e^{\frac{p}{q}}. \tag{15}$$

The stability of the terminal sliding surface in Equation (14) can be analysed through the following CLF:

$$W = \frac{1}{2}e^2. \tag{16}$$

Using Equation (15), the derivative of W can be written and simplified as

$$\dot{W} = -k_1 e^{\frac{p}{q}+1} \leq 0. \tag{17}$$

Equation (17) clearly indicates the stability of the non-singular terminal sliding surface. Therefore, the sliding mode controller designed based on this sliding surface will ensure the convergence of both tracking error and its dynamic to zero.

It can be summarised that the tracking error along with the terminal sliding surface will tend to zero in a finite time in order to ensure the stability of the ASD in RGPDSs. The desired control objective can be achieved if the control law is designed in such a way that it satisfies the stability condition as per the Lyapunov stability theory. At this point, the CLF (W_{NT-SMC}) for ensuring the convergence of the non-singular terminal sliding surface can be considered as follows:

$$W_{NT-SMC} = \frac{1}{2}S^2_{NT-SMC} \tag{18}$$

and its derivative as

$$\dot{W}_{NT-SMC} = S_{NT-SMC}\dot{S}_{NT-SMC} \tag{19}$$

Now, it is essential to take the derivative of S_{NT-SMC} in Equation (14) in order to obtain $\dot{S}_{NT-SMC}$ which can be written as

$$\dot{S}_{NT-SMC} = \ddot{e} + \frac{k_1 p}{q}|e|^{\frac{p}{q}-1}\dot{e} \tag{20}$$

Since $e = i_N - i_{N_{\text{ref}}}$, $\dot{e}$ and $\ddot{e}$ can be written as follows:

$$\begin{aligned} \dot{e} &= \frac{1}{L_p}(mV_{dc} - v_N) - \dot{i}_{N_{\text{ref}}} \\ \ddot{e} &= \frac{1}{L_p}(\dot{m}V_{dc} - \dot{v}_N) - \ddot{i}_{N_{\text{ref}}} \end{aligned} \tag{21}$$

Substitution Equation (21) into Equation (20), Equation (19) can be written as follows:

$$\begin{aligned} \dot{W}_{NT-SMC} = S_{NT-SMC}\Bigg[&\frac{V_{dc}}{L_p}\dot{m} - \frac{\dot{v}_N}{L_p} - \ddot{i}_{N_{\text{ref}}} \\ &+ \frac{k_1 p}{q}|e|^{\frac{p}{q}-1}\left(\frac{V_{dc}}{L_p}m - \frac{v_N}{L_p} - \dot{i}_{N_{\text{ref}}}\right)\Bigg] \end{aligned} \tag{22}$$

The sliding surface will be stable, that is, $dot W_{NT-SMC} \leq 0$ if the following condition is satisfied:

$$\begin{aligned} \Bigg[&\frac{V_{dc}}{L_p}\dot{m} - \frac{\dot{v}_N}{L_p} - \ddot{i}_{N_{\text{ref}}} + \frac{k_1 p}{q}|e|^{\frac{p}{q}-1} \\ &\left(\frac{V_{dc}}{L_p}m - \frac{v_N}{L_p} - \dot{i}_{N_{\text{ref}}}\right)\Bigg] = -k_2 \text{sgn}(S_{NT-SMC}) \end{aligned} \tag{23}$$

where k_2 is a positive gain parameter while sgn represents a signum function expressed as

$$\text{sgn}(S_{NT-SMC}) = \begin{cases} +1 & \text{if } S_{NT-SMC} > 0 \\ 0 & \text{if } S_{NT-SMC} = 0 \\ -1 & \text{if } S_{NT-SMC} < 0 \end{cases} \tag{24}$$

The switching control input ($\dot{m} \equiv \dot{m}_{NT-SMC}$) can be determined from Equation (23) and written as follows:

$$\dot{m}_{NT-SMC} = \frac{L_p}{V_{dc}}\left[\frac{\dot{v}_N}{L_p} + \ddot{i}_{N_{\text{ref}}} - \frac{k_1 p}{q}|e|^{\frac{p}{q}-1} \left(\frac{V_{dc}}{L_p}m - \frac{v_N}{L_p} - \dot{i}_{N_{\text{ref}}}\right) - k_2 \text{sgn}(S_{NT-SMC})\right]. \tag{25}$$

At this point, $\dot{W}_{NT-SMC}$ in Equation (22) can be simplified as

$$\dot{W}_{NT-SMC} = -k_2 S_{NT-SMC}\, sgn(S_{NT-SMC}). \tag{26}$$

The control law in (25) includes a signum function which will introduce chattering into the system response. The chattering problem can be avoided by replacing the signum function with the following continuous function:

$$sgn(S_{NT-SMC}) = \frac{S_{NT-SMC}}{|S_{NT-SMC}| + \epsilon}, \tag{27}$$

where ϵ is a positive constant having a very small value that is used to reduce the chattering problem. Using Equation (27), Equation (26) can be written as

$$\dot{W}_{NT-SMC} = -k_2 \frac{S^2_{NT-SMC}}{|S_{NT-SMC}| + \epsilon} \leq 0, \tag{28}$$

which indicates the overall stability of the ASD and finally, the control input for the RCC inverter in Equation (25) can be written as

$$\dot{m}_{NT-SMC} = \frac{L_p}{V_{dc}}\left[\frac{\dot{v}_N}{L_p} + \ddot{i}_{N_{\text{ref}}} - \frac{k_1 p}{q}|e|^{\frac{p}{q}-1} \left(\frac{V_{dc}}{L_p}m - \frac{v_N}{L_p} - \dot{i}_{N_{\text{ref}}}\right) - k_2 \frac{S_{NT-SMC}}{|S_{NT-SMC}| + \epsilon}\right]. \tag{29}$$

The NT-SMC as represented by Equation (29) is used for the fault current compensation to mitigate powerline bushfires using the RCC inverter with an ASD. It is worth noting that Equation (29) is the designed sliding mode control law. The reachability of this NT-SMC is provided in the Appendix. From Equation (29), it can be seen that the control input will never experience singularity problems as all terms in the denominator (i.e. V_{dc}, q, L_p, and ϵ) are positive definite, that is, greater than 0. The singularity problem basically arises when $|S_{NT-SMC}| = 0$ and ϵ is discrete. However, this is not the case for the newly derived control input in Equation (29). The performance of this controller is compared with an I-SMC to ensure that the comparison is made with a controller that has almost similar features (especially, in terms of design parameters). Since the application of SMCs is relatively new for the control of RCC inverter, the design procedure for the I-SMC is briefly provided in the following subsection.

3.2 | Brief overview of an I-SMC for RCC inverters in ASDs

For the I-SMC, the integral sliding surface is considered as follows:

$$S_{I-SMC} = k_d \dot{e} + e + k_i \int e dt, \tag{30}$$

where k_d and k_i are positive constants which are used to control the convergence speed of the error. As indicated in the previous subsection, the tracking error along with the integral sliding surface will tend to zero and the CLF (W_{I-SMC}) for ensuring the convergence of this sliding surface can be considered as follows:

$$W_{I-SMC} = \frac{1}{2} S^2_{I-SMC}. \tag{31}$$

Similar to the NT-SMC design process, $\dot{W}_{I-SMC}$ can be written as

$$\dot{W}_{I-SMC} = S_{I-SMC} \dot{S}_{I-SMC}. \tag{32}$$

Here, $\dot{S}_{ISMC}$ can be determined from Equation (30) by taking its derivative which can written as

$$\dot{S}_{I-SMC} = k_d \ddot{e} + \dot{e} + k_i e. \tag{33}$$

The substitution of Equation (21) into Equation (33) and finally, Equation (33) into Equation (32) yields

$$\dot{W}_{I-SMC} = S_{I-SMC}\left[k_d\left(\frac{V_{dc}}{L_p}\dot{m} - \frac{\dot{v}_N}{L_p} - \ddot{i}_{N_{\text{ref}}}\right) + \left(\frac{V_{dc}}{L_p}m - \frac{v_N}{L_p} - \dot{i}_{N_{\text{ref}}}\right) + k_i e\right]. \tag{34}$$

The sliding surface will be stable, that is, $\dot{W}_{I-SMC} \leq 0$ if the following condition is satisfied:

$$\left[k_d\left(\frac{V_{dc}}{L_p}\dot{m} - \frac{\dot{v}_N}{L_p} - \ddot{i}_{N_{\text{ref}}}\right) + k_i e + \left(\frac{V_{dc}}{L_p}m - \frac{v_N}{L_p} - \dot{i}_{N_{\text{ref}}}\right)\right] = -\eta \text{sgn}(S_{I-SMC}), \tag{35}$$

where η is a positive gain parameter and the function is similar to that as represented by Equation (24). The switching control input ($\dot{m} \equiv \dot{m}_{I-SMC}$) can be determined from Equation (35) and written as follows:

$$\dot{m}_{I-SMC} = \frac{L_p}{k_d V_{dc}}\left[k_d \frac{\dot{v}_N}{L_p} + k_d \ddot{i}_{N_{\text{ref}}} - k_i e - \left(\frac{V_{dc}}{L_p} m - \frac{v_N}{L_p} - \dot{i}_{N_{\text{ref}}}\right) - \eta \text{sgn}(S_{I-SMC})\right]. \tag{36}$$

At this point, $\dot{W}_{I-SMC}$ in Equation (34) can be written as

$$\dot{W}_{NT-SMC} = -\eta S_{NT-SMC} \text{sgn}(S_{NT-SMC}) \tag{37}$$

The control law in (36) includes a signum function which will introduce chattering into the system response. The chattering problem can be avoided by replacing the signum function with the following continuous function:

$$\text{sgn}(S_{I-SMC}) = \frac{S_{I-SMC}}{|S_{I-SMC}| + \sigma}, \tag{38}$$

where σ is a positive constant having a very small value that is used to reduce the chattering problem. Using Equation (38), Equation (37) can be written as

$$\dot{W}_{I-SMC} = -\eta \frac{S^2_{I-SMC}}{|S_{I-SMC}| + \sigma} \leq 0 \tag{39}$$

which indicates the overall stability of the ASD and finally, the control input for the RCC inverter in Equation (36) can be written as

$$\dot{m}_{I-SMC} = \frac{L_p}{k_d V_{dc}}\left[k_d \frac{\dot{v}_N}{L_p} + k_d \ddot{i}_{N_{\text{ref}}} - k_i e - \left(\frac{V_{dc}}{L_p} m - \frac{v_N}{L_p} - \dot{i}_{N_{\text{ref}}}\right) - \eta \frac{S^2_{I-SMC}}{|S_{I-SMC}| + \sigma}\right]. \tag{40}$$

The NT- and I-SMCs as represented by Equations (29) and (40) are used for compensating the fault current and the performance of these controllers are compared through rigorous simulation results in order to demonstrate the superiority of the NT-SMC over the I-SMC under different fault resistances as discussed in the following section.

4 | CONTROLLER PERFORMANCE EVALUATION

The RGPDS as shown in Figure 1 is considered as the test system to verify the effectiveness of the NT-SMC over the I-SMC. The MATLAB/SIMULINK platform is used to build the system and design both controllers using respective control laws. The parameters of the test system are considered as similar to that as presented in [30]. The test distribution network is considered as a 22 kV (rms) system, that is, the line-to-line voltage is 22 kV (rms) which corresponds to the line- or phase-to-ground voltage as 12.7 kV (rms). At the same time, the phase-to-neutral voltage is also considered as 12.7 kV (rms) as the internal resistance is neglected. The simulation is carried out by considering the value of the adjustable inductor (L_p) as 0.9 H. Since the distribution network is considered as a balanced system, the values of per phase zero-sequence resistance and capacitance are considered as 28 kΩ and 4 μF, respectively; that is, similar to that as presented in [30]. The load resistance between each phase and neutral is considered as 400 Ω. In Figure 1, it can be seen that the T-type RCC inverter uses an 800 V DC source which is split into two 400 V DC sources as the input. Since the phase voltage for the distribution substation in Figure 1 is 12.7 kV and the REFCL is capable to detect the fault current up to 0.5 A, the maximum value of the fault impedance is 25.4 kΩ. Hence, the lowest value of the fault worst value of the fault current is 0.5 A as this cannot be detected through traditional overcurrent relays. Furthermore, the REFCL with an appropriate controller for the RCC inverter provides full compensation of the fault current. The performance of the designed controller is also evaluated through PIL simulations to further verify its effectiveness in the real-time environment.

4.1 | Standard simulations

Simulations studies are performed to demonstrate the compensation of the fault current through the RCC inverter while using the designed NT-SMC for mitigating the devastating consequences of powerline bushfires. The switching control input for the NT-SMC is designed using Equation (29) and an integral action is then applied which is finally fed through a pulse width modulator (PWM) as these switches require pulses. Here, the switching frequency of the RCC inverter to generate switching pulses is considered as 10 kHz and a similar process is followed for the implementation of the I-SMC. The fault current compensation capability of the RCC inverter with the designed controller is verified by analysing the results against the standard operational criteria to mitigate powerline bushfires as presented in [4]. These criteria are set for fault currents with both low and high impedance faults. In this simulation, the high impedance fault is considered as the fault resistance having a value lower than or equal to 1 kΩ, whereas this value is considered as greater than 1 kΩ for high impedance faults. As indicated earlier on, ASDs in RGPDSs are capable to detect a fault with the fault current having a value higher than 0.5 A, that is, for the highest fault impedance of 25.4 kΩ [2]. As per the operational standard in [4], the fault current needs to be compensated in such a way that it becomes below 0.5 A within 2 s after initiating the RCC inverter for both high and low impedance faults. During the practical operation, the ASD generally activates the RCC inverter as soon as the fault is detected for immediately mitigating powerline bushfires. At this instant, the voltage of the faulty phase is also observed at different instances (85 ms, 0.5 s, and 2 s) after initiating the operation of the RCC inverter while fault

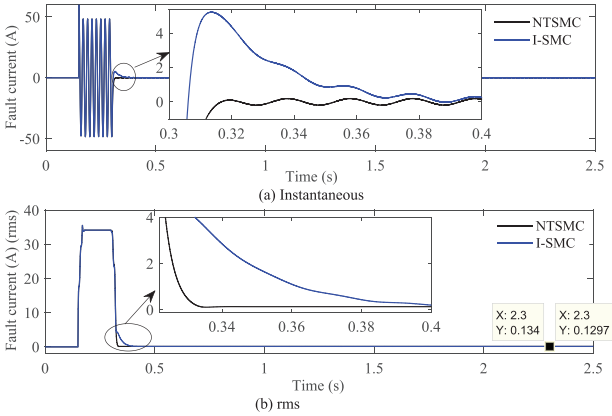

FIGURE 2 Fault current for the operating scenario with R_f =250 Ω and an SLG fault on Phase *B*

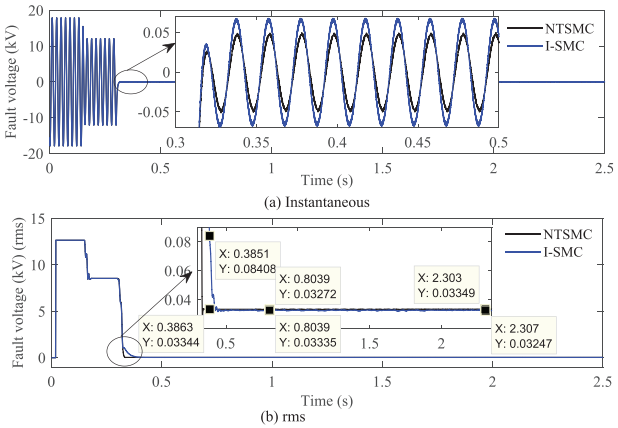

FIGURE 3 Faulty phase voltage for the operating scenario with R_f =250 Ω and an SLG fault on Phase *B*

impedances are low. However, this voltage needs to observe only at 2 s if the fault impedance is high [4]. For both low and high impedance faults, the maximum value of the faulty phase voltage should be kept within 250 V at 2 s after starting the operation of the RCC inverter while this voltage needs to be maintained as 1900 V and 750 V (maximum values) at 85 ms and 0.5 s, respectively, for low impedance faults [4]. The parameters required for the NT-SMC are considered as: $p = 5$, $q = 3$, $k_1 = 8000$, $k_2 = 500$, and $\epsilon = 0.5$ while the parameters for the I-SMC as: $k_d = 500$, $k_i = 9000$, $\eta = 450$, and $\sigma = 0.5$. These parameters are selected based on the design criteria as discussed in Section 3 where it is clearly mentioned that the values of p and q need to be odd numbers and satisfy $q < p < 2q$. It is also mentioned that the values of k need to be high, whereas ϵ and σ should be small to avoid the chattering effects. It is worth noting that these values in this paper are selected using a trial and error method.

The performance of the controller is evaluated by applying a single phase-to-ground fault on Phase *B* by considering both low and high impedance faults. These values are considered as 250 Ω, 900 Ω, and 26 kΩ for which the fault current will vary. The simulations are conducted by activating the RCC inverter after 0.15 s of occurring the SLG fault where it is considered that the fault occurs at $t = 0.15$ s while the RCC inverter is activated at $t = 0.3$ s and the RGPDS is simulated until t=2.5 s, that is, for at least 2 s (actually 2.3 s) after activating the RCC inverter. The remaining of this section includes the detailed discussions on the capability of both NT- and I-SMCs in terms of compensating the fault current.

At the first instance, the RGPDS is simulated for a low impedance fault with R_f=250 Ω and simulation results are analysed through the fault current, faulty phase voltage, and current injection by the RCC inverter. All these responses are presented in Figures 2–4 in their both instantaneous and rms forms. The fault current in Figure 2 clearly shows that both controllers start compensating this as soon as the fault occurs and the RCC inverter is activated. The differences in the performance of NT- and I-SMCs cannot be evidenced from the instantaneous response of the fault current in Figure 2.

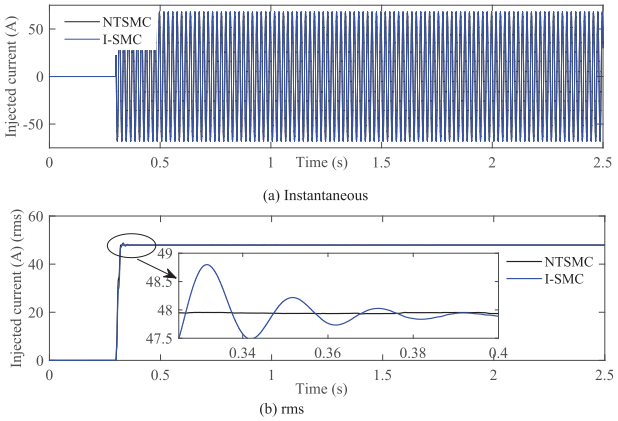

FIGURE 4 Current injected by the RCC inverter for the operating scenario with R_f =250 Ω and an SLG fault on Phase *B*

However, the rms response in the same figure (i.e. Figure 2) shows that the NT-SMC compensates the fault current in a faster way as compared to the I-SMC. Furthermore, the differences in the performance of NT- and I-SMCs can be clearly seen from the expanded version of the fault current response in Figure 2. Both controllers keep the value of the current well below 0.5 A (e.g. 0.1297 A for the NT-SMC and 0.134 A for the I-SMC) within 2 s after starting the RCC inverter. The faulty phase voltage is shown in Figure 3 whose value is observed at 0.385 s, 0.8 s, and 2.3 s (i.e. at 85 ms, 0.5 s, and 2 s after the fault inception) and at these time instances, the value of this voltage is found as around 33.44 V, 33.35 V, and 32.47 V for the NT-SMC while the I-SMC ensures this value as around 84 V, 80.39 V, and 33.5 V. This clearly depicts that both ST- and I-SMCs satisfy the voltage requirement for the faulty phase in order to compensate the fault current in an RGPDS. However, the NT-SMC reduces the faulty voltage much faster than the I-SMC while ensuring a lower value. Hence, the ST-SMC exhibits better fault current compensation capability and this can be further evidenced from Figure 4 which demonstrates the current injected by the RCC inverter. Initially, this inverter does not inject current as the fault occurs at $t = 0.15$ s and the RCC inverter is activated at $t = 0.3$ s.

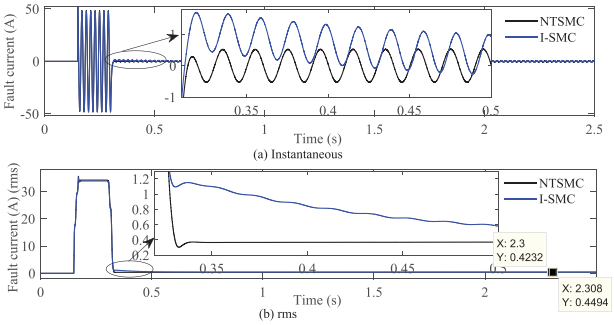

FIGURE 5 Fault current for the operating scenario with $R_f = 250\ \Omega$ and an SLG fault on Phase *B* while subjected to external disturbances and parameter variations

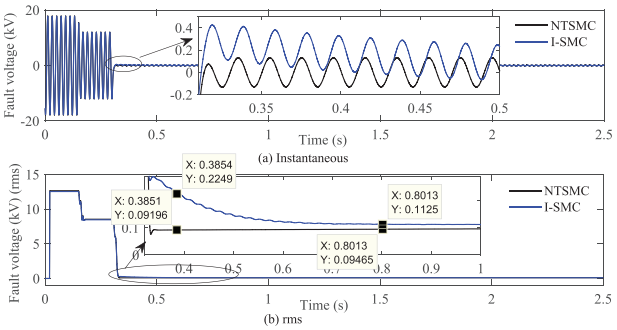

FIGURE 6 Faulty phase voltage for the operating scenario with $R_f = 250\ \Omega$ and an SLG fault on Phase *B* while subjected to external disturbances and parameter variations

However, the current injection by the RCC inverter with both ST- and I-SMCs in Figure 4 clearly shows that the RCC inverter with the NT-SMC injects current in a quicker way than that of the I-SMC which is consistent with the fault current and faulty phase voltage responses.

The performance of the controller is further evaluated for $R_f = 250\ \Omega$ by considering the effects of external disturbances and variations in parameters. During the simulation, the white Gaussian noise having both mean and variation as 0.5 is considered as an external disturbance to the system. Furthermore, the value of L_p is varied by ±30% from its nominal value. The fault current, faulty phase voltage, and current injected by the RCC inverter under this operating condition are shown in Figures 5–7. From these figures, it can be seen that the faulty phase voltage is effectively compensated by the designed NT-SMC and the I-SMC is unable to meet the standard required for the powerline bushfire mitigation though both controllers ensure the desired value of fault current. Furthermore, the injected current by the RCC inverter with the NT-SMC exhibits more stable properties while comparing with that of the I-SMC.

Now, another low impedance fault with R_f=900 Ω is considered for simulating the RGPDS and verifying the effectiveness of the NT-SMC over the I-SMC. Simulation results are presented in terms of similar responses as discussed for low impedance faults, that is, through the fault current, faulty phase voltage, and injected current which are presented in

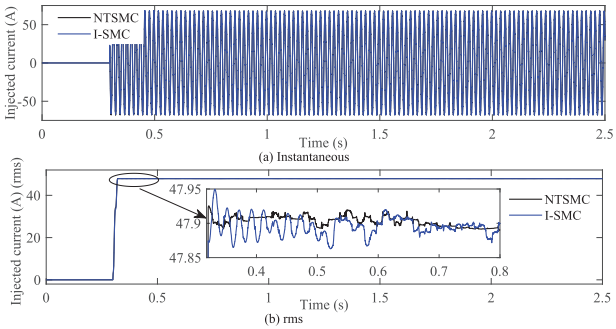

FIGURE 7 Current injected by the RCC inverter for the operating scenario with $R_f = 250\ \Omega$ and an SLG fault on Phase *B* while subjected to external disturbances and parameter variations

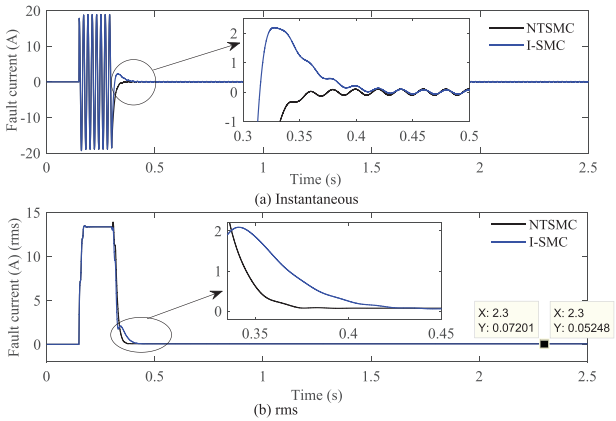

FIGURE 8 Fault current for the operating scenario with R_f =900 Ω and an SLG fault on Phase *B*

Figures 8–10, respectively. It is worth noting that the results are obtained based on similar fault conditions as discussed earlier. The fault current is zero before applying the fault and the system experiences some transients when the fault occurs at $t = 0.15$ s. However, the fault current is compensated by both NT- and I-SMCs which can be clearly seen from Figure 8 where the response time is faster for the NT-SMC

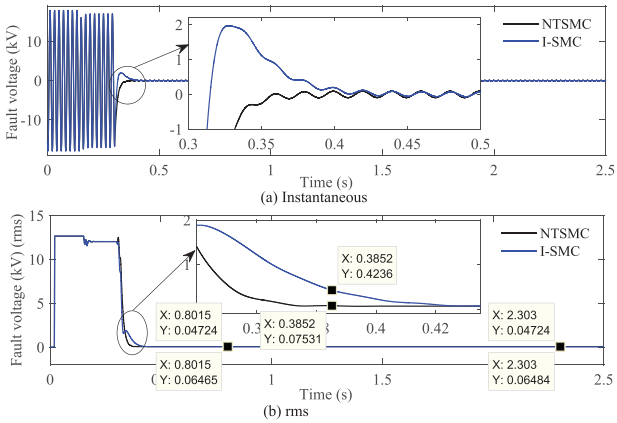

FIGURE 9 Faulty phase voltage for the operating scenario with R_f =900 Ω and an SLG fault on Phase *B*

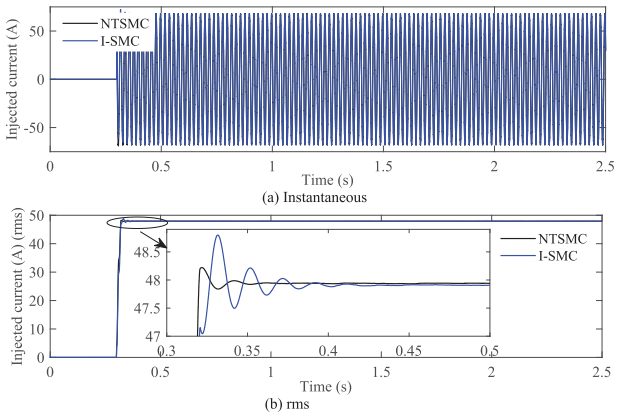

FIGURE 10 Current injected by the RCC inverter for the operating scenario with R_f =900 Ω and an SLG fault on Phase *B*

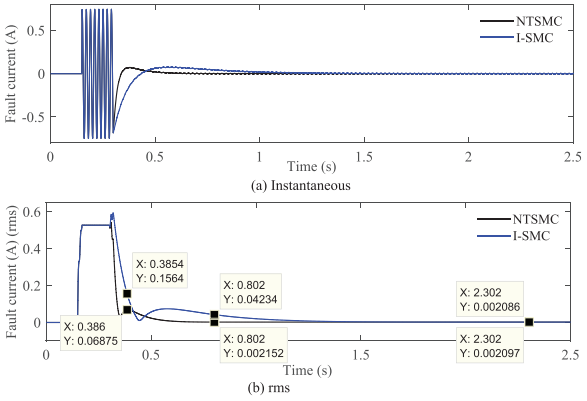

FIGURE 11 Fault current for the operating scenario with R_f = 26 kΩ and an SLG fault on Phase *B*

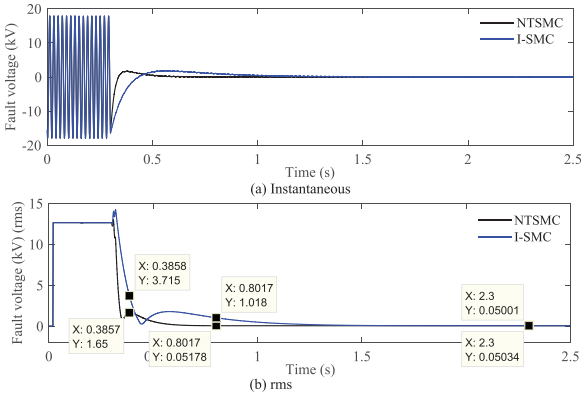

FIGURE 12 Faulty phase voltage for the operating scenario with R_f = 26 kΩ and an SLG fault on Phase *B*

while comparing with the I-SMC. Figure 8 also demonstrates that both controllers ensure the standard operational criteria as discussed in [4] as the fault current is limited to a value significantly lower than 0.5 A within 2 s after starting the operation of the RCC inverter. Actually, the value of the compensated current at t = 2.3 s is 0.05 A with the NT-SMC while it is 0.07 A for the I-SMC. Thus, it can be clearly found that the NT-SMC outperforms the I-SMC in terms of its capability to fully compensate the fault current. The faulty phase voltage in Figure 9 shows that its value is significantly lower than 250 V with both controllers at t = 2.3 s. Actually, the value of the faulty phase voltage at t = 2.3 s is around 50 V when the NT-SMC is used and it becomes 50.34 V if the I-SMC is employed for the RCC inverter though its value is 423.6 V with the I-SMC and 75.31 V with the NT-SMC at t = 0.385 s, that is, at 85 ms after the fault inception. Therefore, the faulty phase voltage aligns with the fault current and the NT-SMC ensures better performance for maintaining the faulty phase voltage while comparing with the I-SMC. The current injection through the RCC inverter is demonstrated in Figure 10 which further verifies the superiority of the NT-SMC over the I-SMC to compensate the fault current due to an SLG fault in an RGPDS. Hence, the NT-SMC enables the RCC inverter to effectively compensate the fault current.

The highest value of the fault resistance, that is, R_f=26 kΩ, is taken into account to further analyse the performance of the NT-SMC under the worst case condition. In this case, simulation results are obtained by considering similar fault conditions and responses of the RGPDS as discussed for other low fault impedances. The comparative study is carried out with an I-SMC where the responses in Figures 11–13 shows almost similar features as discussed for two other fault resistances. The main difference is in the value of the fault current which is significantly lower for this fault impedance and this can be clearly seen from Figure 11. The faulty phase voltage in Figure 12 and the injected current in Figure 13 shows that the NT-SMC ensures better transient characteristics as compared to the I-SMC. Therefore, it can be clearly said that the RCC inverter with both controllers compensates the fault current by appropriately tracking the neutral current and thus, the effects of powerline bushfires are mitigated.

Apart from this, the performance of the designed NT-SMC is compared with a PR controller which is well known for its capability to track the sinusoidal reference. The key findings in terms of maintaining the faulty phase voltage at different time instances with the fault impedances of 250 Ω, 900 Ω, and 26 kΩ

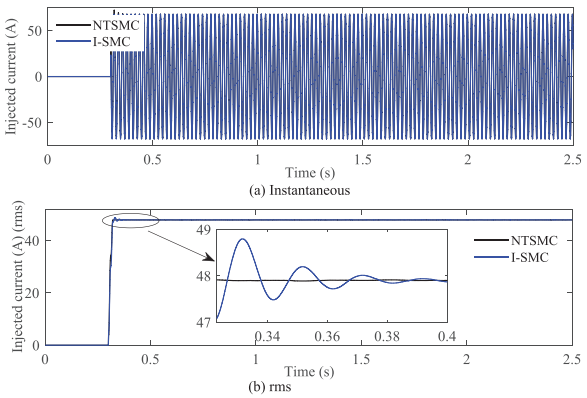

FIGURE 13 Current injected by the RCC inverter for the operating scenario with R_f =26 kΩ and an SLG fault on Phase *B*

TABLE 1 The rms values of the faulty phase voltage with $R_f = 250\ \Omega$

RCC activation time	Simulation time (s)	PR (kV)	I-SMC (kV)	NT-SMC (kV)
85 ms	0.385	0.2478	0.08408	0.03344
0.5 s	0.8	0.03485	0.03335	0.03272
2 s	2.3	0.03450	0.03247	0.03349

TABLE 2 The rms values of the faulty phase voltage with $R_f = 900\ \Omega$

RCC activation time	Simulation time (s)	PR (kV)	I-SMC (kV)	NT-SMC (kV)
85 ms	0.385	0.8949	0.4236	0.07531
0.5 s	0.8	0.04880	0.06465	0.04727
2 s	2.3	0.04750	0.06484	0.04727

are summarised in Tables 1–3, respectively. From these tables, it can be found that the designed NT-SMC outperforms the PR controller for almost all time instances.

4.2 | PIL simulations

The performance of the NBC is evaluated on a real-time platform through the PIL simulation. In this PIL simulation, the control algorithm is executed in a processor where an Arduino MEGA 2560 processor is used and the original system along with the derived control law is in the MATLAB/SIMULINK platform as shown in Figure 14. The same system, as discussed earlier in this section, is used in the MATLAB/SIMULINK platform and the PIL simulation is carried out for all fault impedances as discussed in the previous subsection. However, the results are presented here only for R_f =250 Ω while considering the similar fault sequence. In Figure 14, it can be seen that the control signal derived by using the NT-SMC is fed through the PIL block instead of directly feeding it to the simulation model. The PIL block interfaces the processor (i.e. Arduino MEGA 2560) with the simulation platform. The control signal is then executed in the Arduino MEGA 2560 processor and finally, the control signal generated from this processor is used for the switching signal of the RCC inverter. Hence, therefore, the controller runs in the processor and the control signal generated from this processor work on any system (i.e. physical or simulation models). The fault current, faulty phase voltage, and

TABLE 3 The rms values of the faulty phase voltage with $R_f = 26\ \text{k}\Omega$

RCC activation time	Simulation time (s)	PR (kV)	I-SMC (kV)	NT-SMC (kV)
85 ms	0.385	6.519	3.715	1.65
0.5 s	0.8	0.07152	1.018	0.05178
2 s	2.3	0.0535	0.05034	0.05001

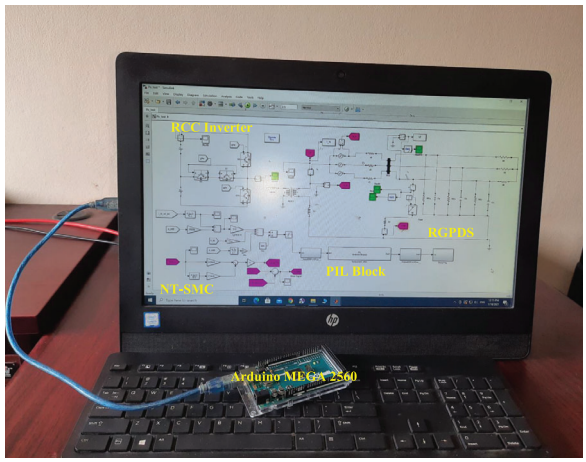

FIGURE 14 PIL simulation setup

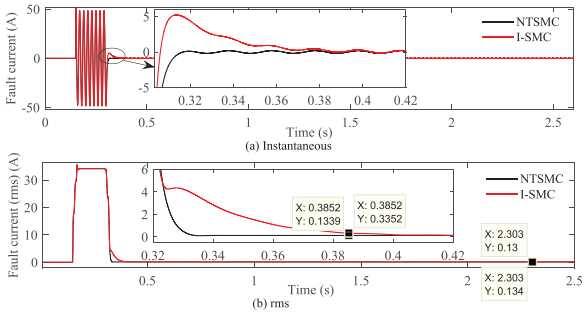

FIGURE 15 Fault current from the PIL simulation for $R_f = 250\ \Omega$

current injected by the RCC inverter are shown in Figures 15–17 which clearly demonstrate that the PIL results are consistent with the simulation results. Hence, the newly designed controller is applicable for the real-time environment.

5 | CONCLUSIONS

The detailed designed procedure of a non-singular terminal sliding mode controller is presented for the residual current compensation inverter used within an ASD in resonant grounded

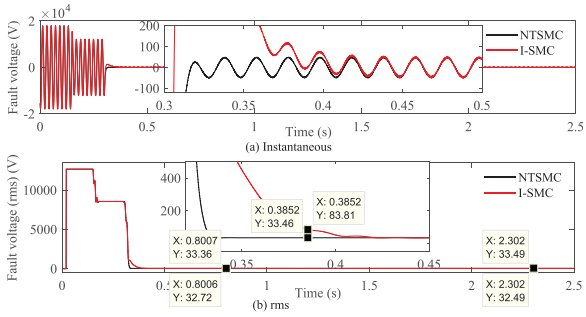

FIGURE 16 Faulty phase voltage from the PIL simulation for $R_f = 250\ \Omega$

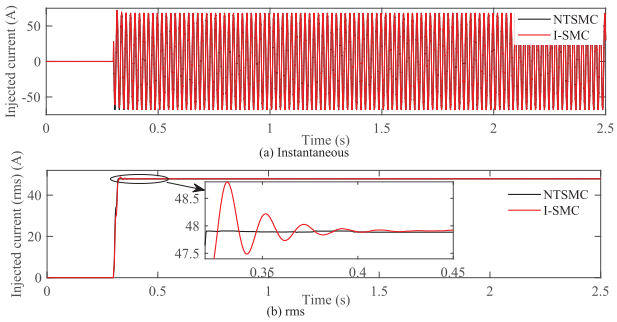

FIGURE 17 Current injected by the RCC inverter from the PIL simulation for $R_f = 250\ \Omega$

power distribution systems. The non-singular terminal sliding mode controller is designed to track the reference value of the neutral current in such a way that the fault current is almost completely compensated which in turn reduces the chances of igniting powerline bushfires. Since the designed nonsingular terminal sliding mode controller is completely new for the fault current compensation, another integral sliding mode controller is also designed to present a comparative study under variation in operating conditions which are depicted through changes in the fault current due to the variation in the fault resistance. Three different operating scenarios are considered to further justify the effectiveness of the designed nonsingular terminal sliding mode controller over the integral sliding model controller. Although there are no significant differences in their performance, the response for the non-singular terminal sliding mode controller is much faster than the integral sliding mode controller. It is worth noting that both controllers satisfy the standard required for the operation of resonant grounded power distribution networks in bushfire prone areas. In future, the works will be directed towards a similar type of fault compensation by considering more operational constraints such as the parametric uncertainty in the value of the adjustable coil and external disturbances (such as harmonics) due to variations in the load demand as well as imbalances in networks. The harmonics in the fault current with different fault resistances will be high even after using the designed controller as the dynamic of the filter is not considered. Future works will also consider appropriate filter design for rejecting harmonics in the fault current.

DATA AVAILABILITY STATEMENT

The data that support the findings of this study are available from the corresponding author upon reasonable request.

ORCID

Tushar Kanti Roy https://orcid.org/0000-0002-1992-0881
Md Apel Mahmud https://orcid.org/0000-0002-5302-5338

REFERENCES

1. IEEE: IEEE recommended practice for grounding of industrial and commercial power systems. IEEE Std 142-2007 (Revision of IEEE Std 142-1991), pp. 1–225. IEEE, Piscataway, NJ (2007)
2. Orton, T.: Powerline Bushfire Safety Taskforce: Final Report. [Final Report]Energy Safe Victoria (2011)
3. Mitolo, M., Musca, R., Tartaglia, M., Zizzo, G.: Electrical safety analysis in the presence of resonant grounding neutral. IEEE Trans. Ind. Appl. 55(5), 4483–4489 (2019)
4. Regulatory Impact Statement: Bushfire Mitigation Regulations Ammendment. Department of Economic Development, Jobs, Transport and Resources (2015)
5. Fangyao Wang, Moufa Guo & Yang, G.: Novel arc-suppression methods based on cascaded H-bridge converter. In: 2016 Asia-Pacific International Symposium on Electromagnetic Compatibility (APEMC), pp. 691–694. IEEE, Piscataway, NJ (2016)
6. Janssen, M., Kraemer, S., Schmidt, R. & Winter, K. Residual current compensation (rcc) for resonant grounded transmission systems using high performance voltage source inverter. In: 2003 IEEE PES Transmission and Distribution Conference and Exposition, pp. 574–578. IEEE, Piscataway, NJ (2003)
7. Qi, M., Leng, H., Zhang, Z., Yang, L., Peng, S. & Zeng, X.: Fast disposal method for reducing electricity risk of single-phase ground fault in distribution network. In: 2017 China International Electrical and Energy Conference (CIEEC), pp. 554–558. IEEE, Piscataway, NJ (2017)
8. Gargoom, A., Barik, M.A., Mahmud, M.A., Haque, M.E., Oo, A.M.T. & Al-Khalidi, H. et al.: Residual current compensator based on voltage source converter for compensated distribution networks. In: 2018 IEEE Power Energy Society General Meeting (PESGM), pp. 1–5. IEEE, Piscataway, NJ (2018)
9. Wang, P., Chen, B., Tian, C., Sun, B., Zhou, M., Yuan, J.: A novel neutral electromagnetic hybrid flexible grounding method in distribution networks. IEEE Trans. Power Delivery 32(3), 1350–1358 (2017)
10. Zheng, Z.Y., Guo, M.F., Yang, N.C., Jin, T.: Flexible arc-suppression method based on improved distributed commutations modulation for distribution networks. Int. J. Electr. Power Energy Syst. 116, 105580 (2020)
11. Zheng, Z.Y., Guo, M.F., Jin, T., Liu, J.H.: Hybrid flexible arc suppression device based on soft grid connection strategy for MV distribution systems. IET Gener., Transm. Distrib. (2021). https://doi.org/10.1049/gtd2.12194
12. Wang, W., Yan, L., Zeng, X., Fan, B., Guerrero, J.M.: Principle and design of a single-phase inverter-based grounding system for neutral-to-ground voltage compensation in distribution networks. IEEE Trans. Ind. Electr. 64(2), 1204–1213 (2017)
13. Qu, Y., Tan, W. & Yang, Y.: H-infinity control theory apply to new type arc-suppression coil system. In: 2007 7th International Conference on Power Electronics and Drive Systems, pp. 1753–1757. (2007)
14. Qiu, W., Guo, M., Yang, G., Zheng, Z.: Model-predictive-control-based flexible arc-suppression method for earth fault in distribution networks. IEEE Access 7, 16051–16065 (2019)
15. Wen Wang, Lingjie Yan, Bishuang Fan & Xiangjun Zeng: Control method of an arc suppression device based on single-phase inverter. In: 2016 International Symposium on Power Electronics, Electrical Drives, Automation and Motion (SPEEDAM), pp. 929–934. IEEE, Piscataway, NJ (2016)
16. Chen, D., Zeng, X., Peng, S., Wang, Y., Wang, Y. & Zhao, Y. et al.: Active inverter device with double closed loop control method for arc suppression in distribution network. In: 2017 China International Electrical and Energy Conference (CIEEC), pp. 549–553. IEEE, Piscataway, NJ (2017)
17. Wang, W., Zeng, X., Yan, L., Xu, X., Guerrero, J.M.: Principle and control design of active ground-fault arc suppression device for full compensation of ground current. IEEE Trans. Ind. Electr. 64(6), 4561–4570 (2017)
18. Mahmud, M.A., Pota, H.R., Hossain, M.J.: Nonlinear current control scheme for a single-phase grid-connected photovoltaic system. IEEE Trans. Sustainable Energy 5(1), 218–227 (2014). https://ieeexplore.ieee.org/document/6620931
19. Mahmud, M.A., Pota, H.R., Aldeen, M., Hossain, M.J.: Partial feedback linearizing excitation controller for multimachine power systems to improve transient stability. IEEE Trans. Power Syst. 29(2), 561–571 (2014). https://ieeexplore.ieee.org/document/6644312
20. Roy, T.K., Mahmud, M.A., Shen, W., Oo, A.M.T.: Nonlinear adaptive excitation controller design for multimachine power systems with unknown stability sensitive parameters. IEEE Trans. Control Syst. Technology 25(6), 2060–2072 (2017). https://ieeexplore.ieee.org/abstract/document/7802589

21. Zheng, Z., Guo, M., Yang, N., Jin, T.: FASD based on BSC method for distribution networks. IET Gener. Transm. Distrib. 13(24), 5487–5494 (2019)
22. Zheng, Z.Y., Guo, M.F., Yang, N.C., Jin, T.: Single-phase flexible arc suppression device based on BSC-SOGI-PLL method for distribution networks. Int. J. Electr. Power Energy Syst. 121, 106100 (2020)
23. Barzegar-Kalashani, M., Tousi, B., Mahmud, M.A., Farhadi-Kangarlu, M.: Non-linear integral higher-order sliding mode controller design for islanded operations of t-type three-phase inverter-interfaced distributed energy resources. IET Gener. Transm. Distrib. 14(1), 53–61 (2020)
24. Feng, Y., Yu, X., Man, Z.: Non-singular terminal sliding mode control of rigid manipulators. Automatica 38(12), 2159–2167 (2002)
25. Chen, S., Lin, F.: Robust nonsingular terminal sliding-mode control for nonlinear magnetic bearing system. IEEE Trans. Control Syst. Technol. 19(3), 636–643 (2011)
26. Mobayen, S., Tchier, F.: A new LMI-based robust finite-time sliding mode control strategy for a class of uncertain nonlinear systems. Kybernetika 51(6), 1035–1048 (2015)
27. Mofid, O., Mobayen, S., Khooban, M.H.: Sliding mode disturbance observer control based on adaptive synchronization in a class of fractional-order chaotic systems. Int. J. Adapt. Control Signal Process. 33(3), 462–474 (2019)
28. Vaseghi, B., Pourmina, M.A., Mobayen, S.: Finite-time chaos synchronization and its application in wireless sensor networks. Trans. Inst. Meas. Control 40(13), 3788–3799 (2018)
29. Hashemi, S., Pourmina, M.A., Mobayen, S., Alagheband, M.R.: Design of a secure communication system between base transmitter station and mobile equipment based on finite-time chaos synchronisation. Int. J. Syst. Sci. 51(11), 1969–1986 (2020)
30. Roy, T.K., Mahmud, M.A., Nasiruzzaman, A.B.M., Barik, M.A., Oo, A.M.T.: A non-singular fast terminal sliding mode control scheme for residual current compensation inverters in compensated distribution networks to mitigate powerline bushfires. IET Gener. Transm. Distrib. 15(9), 1421–1434 (2021)
31. Roy, T.K., Mahmud, M.A., Ghosh, S.K., Pramanik, M.A.H., Kumar, R. & Oo, A.M.T.: Design of an adaptive sliding mode controller for rapid earth fault current limiters in resonant grounded distribution networks to mitigate powerline bushfires. In: 2021 IEEE Texas Power and Energy Conference (TPEC), pp. 1–6. IEEE, Piscataway, NJ (2021)

How to cite this article: Roy, T.K., Mahmud, M.A. Fault current compensations in resonant grounded distribution systems to mitigate powerline bushfires using a nonsingular terminal sliding model controller. IET Gener. Transm. Distrib. 2021;1–13. https://doi.org/10.1049/gtd2.12294

APPENDIX: REACHABILITY ANALYSIS FOR THE NT-SMC

At the beginning, let assume that S_{NT-SMC} reaches to zero, that is, $S_{NT-SMC} = 0$ from $S_{NT-SMC} \neq 0$ at time, $t = t_r$ and becomes $S_{NT-SMC} = 0$ at $t > t_r$. Thus, once S_{NT-SMC} reaches to zero, it will remain at zero based on the negative semi-definiteness of the derivative of the control Lyapunov function (W_{NT-SMC}) and the tracking error (e) will converge to zero in a finite time, t_s. The total time required from $S_{NT-SMC}(0) \neq 0$ to $e(t_s)$ can be calculated by setting $S_{NT-SMC} = 0$ for which it can be written as

$$\dot{e} = -k_1 e^{\frac{p}{q}}. \tag{A1}$$

The integral of this equation between t_r and t_s can be obtained as

$$\int_{t_r} t_s dt = -\frac{1}{k_1} \int_{t_r} t_s e^{-\frac{p}{q}} de, \tag{A2}$$

which can be simplified as

$$t_s - t_r = -\frac{q}{k_1(q-p)} \left[e(t_s)^{\frac{q-p}{q}} - e(t_r)^{\frac{q-p}{q}} \right]. \tag{A3}$$

Since $e(t_s) = 0$ at $t = t_s$, Equation (A4) can be modified as follows:

$$t_s = t_r + \frac{q}{k_1(q-p)} e(t_r)^{\frac{q-p}{q}} \tag{A4}$$

with $t_r \leq \frac{S_{NT-SMC}(0)}{k_1}$. Hence, it is confirmed that both tracking error (e) and its derivative will converge to zero in a finite time with the NT-SMC.